Identification of Circulating Fibrocytes and Dendritic Derivatives in Corneal Endothelium of Patients With Fuchs' Dystrophy

An-Katrien De Roo,[1,2] Jasper Wouters,[2] Olivier Govaere,[1,3] Beatrijs Foets,[4,5] and Joost J. van den Oord[1,2]

[1]Department of Imaging & Pathology, Laboratory for Translational Cell & Tissue Research, KU Leuven – University of Leuven, Leuven, Belgium
[2]Department of Pathology, UZ Leuven – University Hospitals Leuven, Leuven, Belgium
[3]Institute of Cellular Medicine, Newcastle University, Newcastle upon Tyne, United Kingdom
[4]Department of Ophthalmology, UZ Leuven – University Hospitals Leuven, Leuven, Belgium
[5]Department of Neurosciences, Research Group Ophthalmology, KU Leuven – University of Leuven, Leuven, Belgium

PURPOSE. Fuchs' endothelial corneal dystrophy (FECD) is a degenerative eye disorder affecting 4% of Americans older than 40. It is the leading indication for corneal endothelial (CE) transplantation for which there is a global donor shortage. This study aimed to gain further insight into the pathophysiology of FECD and identify targets for nonsurgical therapy.

METHODS. CE from patients with late-onset FECD was compared with that of normal controls using microarray expression analysis ($n = 4$ FECD, $n = 4$ normal), reverse transcriptase quantitative PCR ($n = 9$ FECD, $n = 8$ normal), and immunohistology ($n = 55$ FECD, $n = 15$ normal).

RESULTS. This led to the identification of circulating fibrocytes and their dendritic derivatives in all examined CE samples with FECD (in all clinical stages of symptomatic FECD and independent of prior cataract surgery). These cells were not present in normal CE. In this study we characterize their morphology, protein expression profile, number, and localization within the CE layer of patients with FECD.

CONCLUSIONS. Circulating fibrocytes and their dendritic derivatives are a new aspect of FECD that deserves further investigation. Because they are known to cause fibrosis in a variety of organs, they may play a similar role in FECD and might be a valuable target for nonsurgical therapy.

Keywords: Fuchs' endothelial corneal dystrophy, circulating fibrocytes, dendritic cells, fibrosis, epithelial-mesenchymal transition

Fuchs' endothelial corneal dystrophy (FECD) is a degenerative corneal disorder that is estimated to affect 4% of Americans older than 40.[1] The exact incidence is unknown because symptomatic FECD is preceded by an asymptomatic phase that does not always evolve into symptomatic disease.[1,2] In the asymptomatic phase (i.e., clinical stage I)[2] corneal guttae develop, which are drop-like excrescences of extracellular matrix (ECM) on the Descemet membrane (DM). Symptomatic progression occurs during the course of 2 to 3 decades.[3] Although an early-onset form of FECD exists (manifesting in the 2nd to 3rd decade of life), this form is very rare.[1] The current study included only late-onset cases of FECD (manifesting in the 5th to 6th decade of life).[3]

FECD usually affects both eyes and clinically progresses from blurred vision to painful erosions and even blindness.[1,4] The blurred vision is caused by corneal swelling as a result of a defect in the inner corneal layer, that is, corneal endothelium (CE).[1,4] CE is derived from the neural crest (not related to vascular endothelium).[5] Normal CE is a monolayer of hexagonal cells in postmitotic arrest that rest on the DM.[6] Normal CE acts as a selective barrier and active pumping system for water and nutrients across the avascular cornea, safeguarding corneal transparency.[1,4] In FECD, CE function is impaired as a result of a critical loss of CE cells (CECs) and thickening of the DM with the appearance of guttae.[1,4]

FECD displays a high familial risk and can be inherited in an autosomal dominant-like way, but most cases are sporadic.[4,7] Smoking is a risk factor and women are 2.5 to 3.5 times more frequently affected than men.[1,4,8] Several mutations, sequence variants, and chromosomal loci have been linked to FECD,[1,4,9,10] but each of those accounts for only a subpopulation of patients. Cellular functions that play a role in FECD include ECM deposition, oxidative stress, apoptosis, and epithelial-mesenchymal transition (EMT),[1,4,9,11,12] but a unifying theory is lacking.

FECD is the leading indication for transplantation of the CE in the United States.[13] Given the global shortage of donor corneas and the expected rise in prevalence of FECD with the aging of the population, this study aimed to gain more insight into the pathophysiology of FECD to identify targets for nonsurgical therapies.[1,14]

MATERIALS AND METHODS

Acquisition of Human Samples and Study Approval

Fresh "CE-DM complexes" (CE monolayers with DM) were prospectively collected from patients with symptomatic late-onset FECD (clinical stages II to IV)[2] during endothelial keratoplasty (CE transplantation). The diagnosis of FECD was made by corneal specialists, based on clinical history, split-lamp biomicroscopic examination (bilateral presence of central guttae with or without edema), and disease progression and excluding other intraocular pathologies (such as uveitis or other inflammatory eye conditions). Patients with previous intraocular surgery other than cataract surgery were excluded from this study. Controls originated from donor corneas and enucleations for uveal melanoma (without corneal extension or prior radiotherapy). The retrieval of donor corneas was performed according to the European Eye Bank Association guidelines, within an average of 6 hours of warm ischemia or 14 hours of cold ischemia. Prior to transplantation and CE-DM collection, donor corneas were stored by organ culture in Stem Alpha medium (Stem Alpha, Saint-Genis-l'Argentière, France), Eurobio medium (Eurobio, Les Ulis, France), or minimal essential medium supplemented with calf serum and antibiotics; dextran was added to reduce swelling prior to transplantation.

This material was either collected in RNA*later* (Ambion by Life Technologies, Carlsbad, CA, USA or Qiagen) for RNA extraction or mounted on tissue slides, with CE facing up, for whole-mount staining. Some samples were partitioned and mounted on multiple slides to enable multiple stains for the same sample (these samples were counted only once to calculate the total number of samples for immunohistochemistry (IHC) and immunofluorescence (IF) and to calculate patient characteristics). Slides were air dried, fixed in acetone, and stored at −20°C.

This study included only residual human material and was approved by the local institutional ethics committee and biobank of UZ Leuven (Commissie Medische Ethiek UZ KU Leuven/Onderzoek; study number S55133) in adherence with the tenets of the Declaration of Helsinki.

RNA Extraction for Microarray Expression Analysis and Reverse Transcription Quantitative Real-Time PCR

CE-DM complexes were manually homogenized with a disposable pestle. RNA extraction was performed with an RNeasy Micro Kit (Qiagen) without DNase treatment (to maximize RNA yield).

Microarray Expression Analysis

Eight RNA samples were selected for microarray expression analysis: four FECD (age 75.5 [4.0], mean [standard deviation] in years; female:male [F:M] ratio 3:1) and four normal control samples (age 52.8 [18.8]; F:M ratio 0:4). RNA concentration and quality was measured using spectrophotometry (NanoDrop ND-1000, Thermo Scientific, Waltham, MA, USA). RNA integrity ranged between 6.70 and 7.90, as measured with a Bioanalyzer 2100 (Agilent, Santa Clara, CA, USA). For each sample, 100 ng of total RNA was spiked with bacterial poly-A RNA positive controls (Affymetrix, Santa Clara, CA, USA) and used to generate second-cycle cDNA with the Ambion WT Expression Kit. Samples were fragmented and biotin-labelled using the Affymetrix WT Terminal Labeling Kit. A mixture of fragmented biotinylated cDNA and hybridization controls (Affymetrix) was hybridized on Affymetrix GeneChip Human Gene 1.0 ST Arrays, followed by staining and washing in a GeneChip fluidics station 450 (Affymetrix). Chips were scanned using a GeneChip scanner 3000 (Affymetrix) to assess the raw probe signal intensities.

MEA was completed in the R programming environment with Bioconductor packages (http://www.bioconductor.org, in the public domain). The analysis was based on the robust multiarray average expression levels of the probe sets with the package xps (version 1.7.2). Probe sets with ≥ 1 present detection call above background were taken into account for further analysis (27,818 probe sets). The average number of present calls per sample was 26,342 (91.2%), with a standard deviation of 416 (1.4%), and comparable average background and scaling factors across the slides. Differential expression was assessed via the moderated t statistic.[15] To control the false discovery rate (FDR), multiple testing correction was performed.[16]

Pathway and function analysis was completed using Ingenuity Pathway Analysis version 8.5-2803 (IPA; Qiagen, Redwood City, CA, USA), with all 27,818 probe sets as input. Of the entries, 19,254 could be mapped to molecules in the Ingenuity Knowledge Base. Probes with $|\log_2 (\text{FECD/normal})| \geq 1$ and FDR-corrected P value < 0.05 were selected. Probe sets referring to the same molecule were resolved by taking the average of the log-ratio values. This resulted in 617 eligible molecules for gene networks and 628 for functions, pathways, and lists.

Reverse Transcription Quantitative Real-Time PCR (RT-qPCR)

Two Custom RT² Profiler PCR Arrays (CAPH10409 and CAPH104010; Qiagen) were designed, comprising 197 genes of interest based on MEA data: 85 fulfilled the cut-off criteria $|\log_2 (\text{FECD/normal})| \geq 1$ and FDR-corrected P value < 0.05; 94 genes were added to complement the pathways of interest, as identified by IPA. RNA concentration and quality was measured using spectrophotometry (NanoDrop ND-1000). Nine unpooled FECD (age 67.8 [8.0]; F:M ratio 5:4) and eight unpooled normal control samples (age 59.6 [12.3]; F:M ratio 2:6), different from those used for MEA, were analyzed with RT-qPCR. Five of 9 FECD samples and seven of eight normal samples contained enough mRNA to be used on both arrays; the other samples were used on one array each. Per array, 100 ng of total RNA was reverse transcribed to cDNA with the RT² First Strand Kit (Qiagen). Arrays were run on the 7900 HT Fast Real-Time PCR System (Applied Biosystems) using RT² SYBR Green ROX qPCR Mastermix (Qiagen).

Data analysis was performed through the web portal of Qiagen (http://qiagen.com/geneglobe, in the public domain). The software performed comparative threshold cycle calculations on the uploaded raw threshold cycle (Ct) data. Normalization was done using the average arithmetic mean of Ct values from three reference genes (*RPL13A*, *RPL19*, and *RPS5*) that were stably expressed in FECD and normal control samples. Ct cut-off was set to 35. Higher Ct values and missing values were imputed with a Ct value of 35. A 2-sided t statistic was used ($\alpha = 0.05$).

Immunostaining on Whole-Mount Specimens

Staining was performed manually or in an automated way with a BOND-MAX stainer (Leica Microsystems, Wetzlar, Germany) or a Link 48 (Dako, Glostrup, Denmark) using diaminobenzidine (brown), alkaline phosphatase (red), or amino-ethylcarbazole (red) as chromogens. Prior to staining with the peroxidase substrates (diaminobenzidine and amino-ethylcarbazole), endogenous peroxidase activity was blocked with

Peroxidase Blocking Solution (Dako) for 10 minutes at room temperature. Pretreatment, dilution, and incubation conditions (Supplementary Table S1) were optimized on fresh-frozen positive control specimens that also served as batch controls. Horseradish peroxidase-labelled EnVision FLEX (Dako) or Bond Polymer Refine Red Detection (Leica) were used as a secondary antibody for 30 minutes. Sections were counterstained with hematoxylin and mounted.

IF double staining consisted of combinations of antisera from different hosts (mouse and rabbit) and goat-anti-mouse or goat-anti-rabbit antibodies labelled with Alexa Fluor 488 or Alexa Fluor 568 (Invitrogen by Life Technologies) as secondary antibodies. Dye swaps ensured the specificity of staining. Slides were counterstained with DAPI (Invitrogen) and mounted with glycerol gelatin or ProLong Gold antifade reagent (Life Technologies).

In total, 55 CE-DM samples from patients with FECD (age 70.1 [8.14]; F:M ratio 36:19) and 15 normal control samples (age 60.1 [15.8]; F:M ratio 10:5) were tested with IHC and IF.

Image Acquisition and Processing

Brightfield images were acquired with a NanoZoomer 2.0-RS (Hamamatsu, Hamamatsu City, Japan), Ultra Fast Scanner 1.6 IVD (Philips, Amsterdam, Netherlands), or DM LB microscope with DC300 camera and IM50 software (Leica). Sample surfaces were calculated with an NDP viewer 2.2.10 (Hamamatsu), IntelliSite Pathology Solution IMS 2.3 (Philips), or Fiji[17] (ImageJ 1.48c; ImageJ, Madison, WI, USA), respectively. Images acquired with the Leica microscope were white balanced, matched for brightness, and corrected with a flatfield background image using EZ Image Prep from ChromaCal Image Calibration 2.5.1 (Datacolor, Lawrenceville, NJ, USA).

IF images were acquired in z-stack using the Leica SP8x confocal microscope. Fiji was used to improve contrast, merge color channels, project the maximum intensity in two dimension, and define scale bars.[17]

The number of immunoreactive cells was counted manually for each marker on the entire sample surface using VersaCount 1.02.[18] Dot plots with 95% confidence intervals were created with GraphPad Prism 6.01 (GraphPad, San Diego, CA, USA). The average number of cells expressing a specific marker was weighted per mm^2 to account for differences in sample surface and for partitioned samples. Cells were manually mapped on whole-slide images and summarized schematically (see Fig. 6). Double-stained samples were counted separately for each of the applied antisera.

RESULTS

Genes Related to Inflammation, Antigen Presentation, and Dendritic Cell Maturation Are Significantly Differentially Expressed in FECD

MEA was used to compare the corneal endothelial transcriptome of four FECD and four normal control samples. For this, RNA was extracted from CE-DM complexes, which contain only CECs, allowing a reliable comparison of the gene expression profiles. Unsupervised computational analysis clearly segregated FECD samples from normal donor samples (Fig. 1a), indicating a marked difference in the gene expression between both groups. This experiment revealed 954 significantly differentially expressed probe sets (487 probe sets were ≥ twofold upregulated and 467 were ≥ twofold downregulated in FECD with an FDR-corrected $P < 0.05$).

IPA analysis of the MEA data indicated a role for functions that are currently not linked to the pathophysiology of FECD,

such as inflammatory response, inflammatory disease, and antigen presentation (Supplementary Fig. S1, Supplementary Table S2). Notably, one of the top gene networks was centered on upregulation of major histocompatibility complex (MHC) class II molecules related to antigen presentation (Fig. 2), with major histocompatibility complex, class II, DR alpha (*HLA-DRA*) being the second most upregulated gene in FECD (fold regulation = 73.95, $P < 0.001$). The most significant canonical pathways included dendritic cell maturation; role of macrophages, fibroblasts, and endothelial cells in rheumatoid arthritis; and hepatic fibrosis/hepatic stellate cell activation (Supplementary Fig. S1, Supplementary Table S2). Note that hepatic stellate cells are a subset of myofibroblasts that play a role in fibrotic liver disorders.[19] Gene set enrichment analysis (Supplementary Methods) confirmed the significant upregulation of genes related to dendritic cell maturation (Fig. 1d, Supplementary Fig. S1).[20]

In addition, MEA revealed biological functions ($P < 0.001$) that are consistent with previously reported processes in FECD (Supplementary Table S2), supporting the external validity of this experiment. These functions included connective tissue development and function (FECD is characterized by ECM deposition),[1] posttranslational modification and free radical scavenging (unfolded protein stress and oxidative stress play a role in FECD),[1,9] cell cycle and cell death (senescence and aberrant apoptosis of CECs have been reported in FECD),[1,4] and nervous system development and function (CE originates from the neural crest).[5]

### RT-qPCR Provides Technical and Biological Validation of the MEA Results

We used RT-qPCR to validate the MEA results on a new and larger set of unpooled samples ($n = 9$ FECD, $n = 8$ normal). For this, we selected 179 genes of interest based on their MEA expression values and role in MHC class II type antigen presentation, dendritic cell maturation, inflammation, chemotaxis, growth factor activity, EMT, and ECM production.

The RT-qPCR results correlated strongly with the MEA results ($R^2 = 0.82$, $P < 0.0001$, Fig. 1c), and unsupervised clustering could again segregate FECD from normal samples (Fig. 1b).

MEA and RT-qPCR data have been deposited in NCBI's Gene Expression Omnibus[21] and are accessible through the Gene Expression Omnibus Series accession number GSE75676 (https://www.ncbi.nlm.nih.gov/geo/query/acc.cgi?acc=GSE75676, in the public domain).

Whole-Mount Staining of CE-DM Complexes Identifies the Presence of Cells With Dendritic and Monocyte-Like Phenotype in FECD

As *HLA-DRA* was one of the top upregulated genes in FECD, according to MEA (fold regulation = 73.95, $P < 0.001$), which was confirmed by RT-qPCR (fold regulation = 169.07, $P = 0.009$), IHC was performed for the HLA-DR α chain (HLA-DRA) on CE-DM whole mounts. Surprisingly, this revealed the presence of HLA-DRA$^+$ cells with dendritic morphology in all of the examined FECD specimens (Fig. 3b), but in none of the controls (Fig. 3a). Another marker related to antigen presentation, namely CD45 (marker of hematopoietic cells),[22] unveiled two subsets of cells, that is, cells with dendritic morphology and moderate CD45 expression, and a smaller subset of monocyte-like cells with bean-shaped nuclei, strong CD45 expression, and lacking dendritic processes (Fig. 3c). IF double staining for CD45 and α smooth muscle actin (αSMA; mesenchymal marker, and marker of EMT; Fig. 4c), HLA-DRA
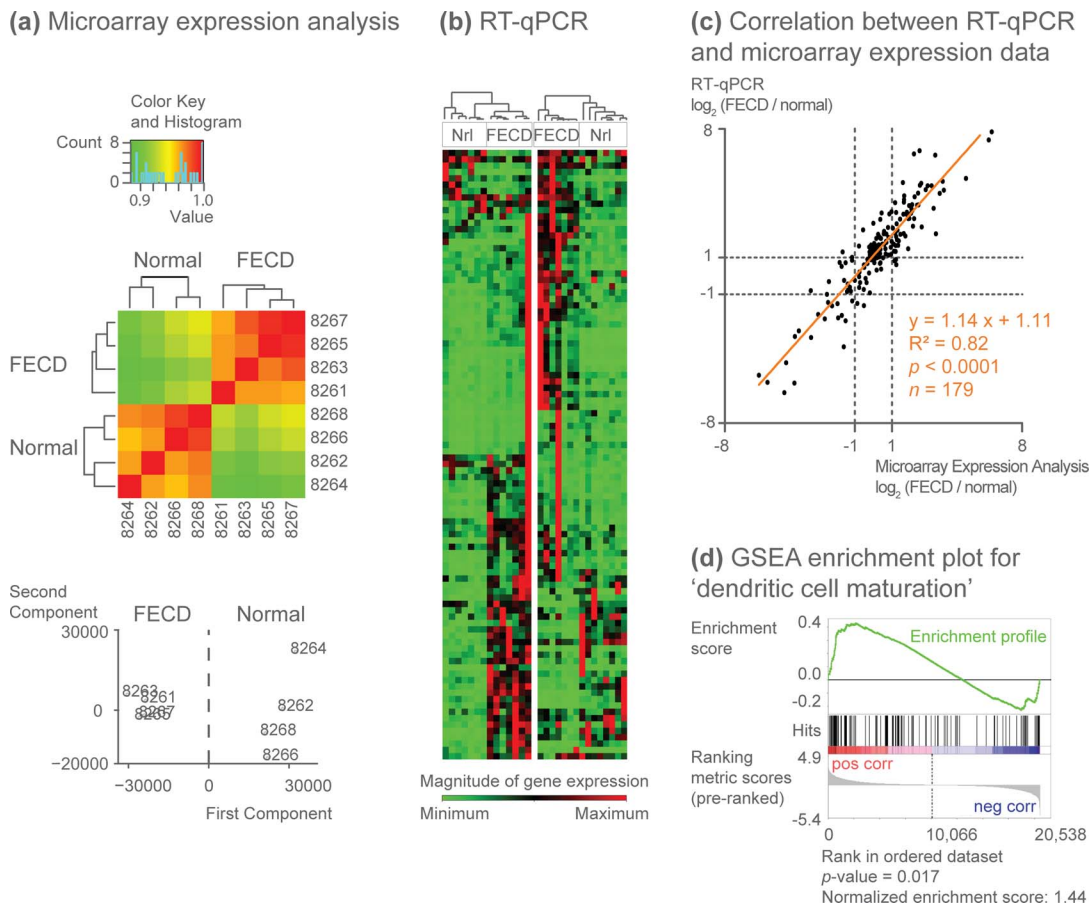
FIGURE 1. Unsupervised computational analysis of MEA and RT-qPCR data segregates FECD from normal control samples. (**a**) The heatmap and cluster analysis (*top*) of MEA data segregated FECD (8261, 8263, 8265, and 8267) from normal control samples (8264, 8262, 8266, and 8268). *Red* indicates similarity between samples. *Green* indicates dissimilarity between samples. The principal component analysis (*bottom*) segregated FECD from normal control samples, with FECD samples clustering together for both components. (**b**) The heatmap and cluster analysis of RT-qPCR data (CAPH10409 array on the *left*, CAPH10410 array on the *right*) segregated FECD from normal control samples (Nrl). Rows correspond to genes, columns correspond to samples. (**c**) The scatterplot with linear regression equation, goodness of fit (R^2), *P* value and number of genes (*n*), indicates a strong correlation between RT-qPCR and MEA results. (**d**) The gene set enrichment analysis (GSEA) of preranked MEA data illustrates the significant upregulation (peak at the beginning of the enrichment profile, positive normalized enrichment score, and $P < 0.05$) for dendritic cell maturation, a canonical pathway identified by IPA analysis (Supplementary Fig. S1). Pos corr: upregulated in FECD versus normal (*red*). Neg corr: downregulated in FECD versus normal (*blue*).

and αSMA (Fig. 4d), as well as HLA-DRA and CD45 (Fig. 5a) showed coexpression of each of these marker pairs within cells with dendritic morphology. In addition, αSMA diffusely stained the CE layer in FECD (Fig. 3f).

Notably, IHC staining for HLA-DRA and CD45 on transversal sections of full-thickness corneas was not suited to demonstrate the presence of cells with dendritic or monocyte-like morphology in FECD. This was a result of sampling bias (for the monocyte-like subset) and the long and slender dendritic processes with scant cytoplasm that only occasionally presented as small dots and were easily overlooked (for the dendritic subset). Transversal staining for αSMA, on the other hand, confirmed a general upregulation of this protein in the CE layer of patients with FECD.

Immunofluorescent Double Staining of CE-DM Complexes Identifies Circulating Fibrocytes in FECD

Next, we aimed to identify the origin and nature of the dendritic and monocyte-like subsets of cells in FECD: either they are derived from CECs (through the process of EMT) or

they are a different cell type that has thus far not been described in FECD. Although the expression of αSMA is compatible with EMT, the expression of CD45 (a specific marker for cells of hematopoietic origin that cannot be obtained by cells of another lineage, not even during the process of EMT)[22-24] pleads strongly against CE origin. Furthermore, these observed bean-shaped nuclei are typical for cells from the monocyte-lineage.

IF double staining for CD34 and collagen I (Fig. 4a) and for CD45 and collagen I (Fig. 4b) revealed coexpression of both marker pairs within cells with monocyte-like morphology. This coexpression profile is the specific signature of circulating fibrocytes. Circulating fibrocytes are bone marrow–derived cells that coexpress hematopoietic markers (such as CD34 and CD45) and mesenchymal markers (such as collagen I)[25] and that are derived from the monocyte/macrophage lineage (with characteristic bean-shaped nuclei). They can differentiate into a variety of phenotypes related to their mixed hematopoietic character (cytokine producing or antigen presenting [HLA-DRA$^+$]) and mesenchymal character (ECM producing [αSMA$^+$]).[25] During this differentiation they can lose surface markers such as CD34 and CD45.[26,27] In our study, cells with dendritic morphology indeed displayed less CD45 and CD34
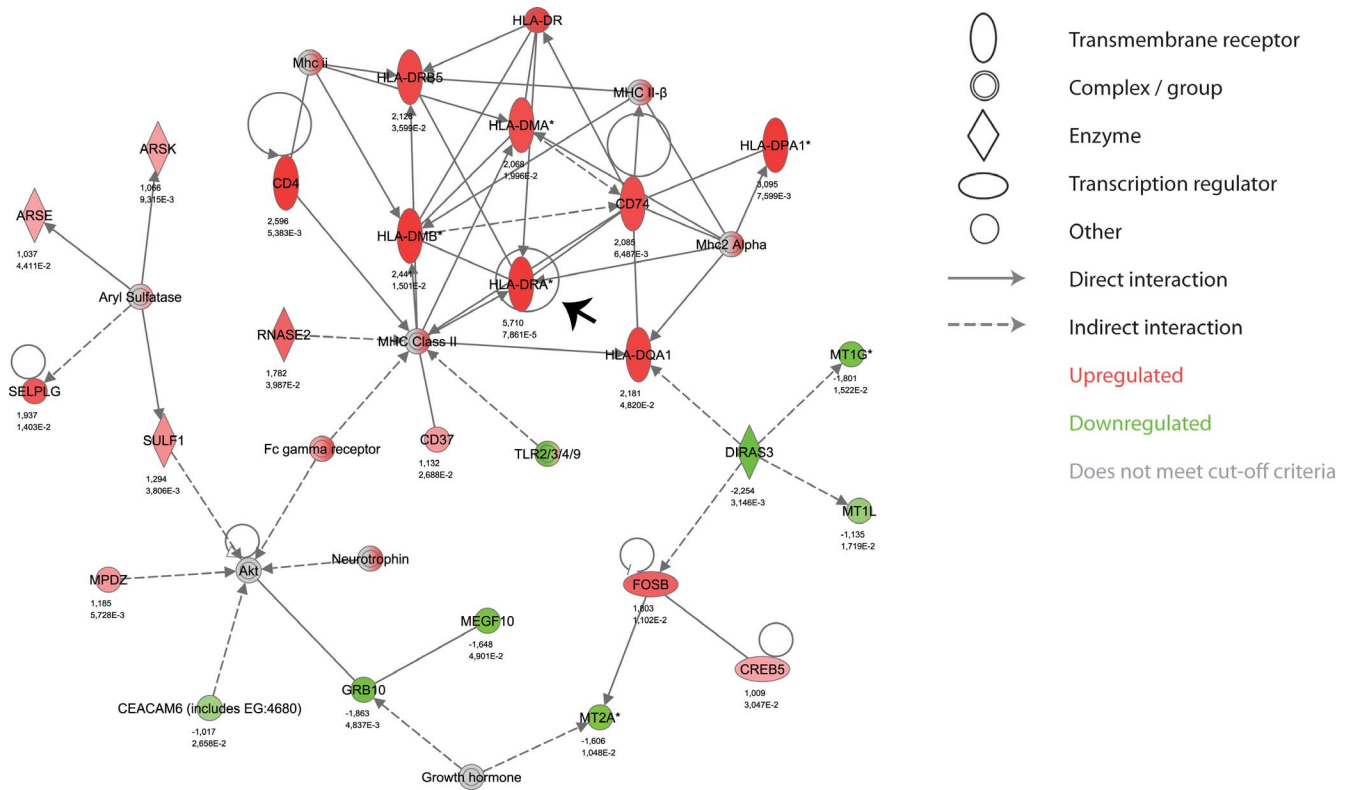
FIGURE 2. Gene network comprising MHC class II molecules is significantly upregulated in FECD. This IPA gene network, based on MEA results, is composed of the functions antigen presentation, inflammatory response, and cell-to-cell signaling and interaction ($P < 0.001$; Supplementary Fig. S1). It shows significant upregulation of _HLA-DRA_ (_arrow_) and other MHC class II molecules. _Red_: $\geq$ 2-fold upregulated (FDR corrected $P < 0.05$). _Green_: $\geq$ 2-fold downregulated (FDR corrected $P < 0.05$). _Gray_: present as input, but not meeting cut-off criteria for _red_ and _green_. The color intensity correlates with the degree of gene expression change. Log$_2$ fold-change values and FDR-corrected P values are below each molecule.

and more HLA-DRA and αSMA (myofibroblast marker; Figs. 3c, 4c, 5a–e, 6a), suggesting a more differentiated stage.

Morphology, Expression Profile, Number, and Localization of Circulating Fibrocytes/Dendritic Derivatives in FECD

To characterize the circulating fibrocyte phenotype in FECD, we applied a set of 18 markers on CE-DM whole mounts from 55 patients with FECD (clinical stages II to IV)[2] and 15 normal controls using either IHC (one marker per slide) or IF double staining (two markers per slide; Figs. 3–6). From the 55 FECD samples, 48 were used to test markers of circulating fibrocytes. Four of these 48 samples originated from phakic eyes (two male and two female patients).

These markers included antibodies to CD11b (marker for precursors of circulating fibrocytes); CCR5, CXCR1, CXCR2, and CXCR4 (chemokine C-C and C-X-C motif receptors involved in recruitment of circulating fibrocytes) and matrix metallopeptidase 9 (MMP9; which is used by circulating fibrocytes to enter the target tissue). Staining for fibronectin ($n = 1$) and vimentin ($n = 1$), two other markers of circulating fibrocytes, proved not useful as both markers also stained CECs (Supplementary Fig. S2). Indeed, fibronectin is overexpressed in CECs with FECD,[28] and vimentin is a marker of normal CECs.[29] Furthermore, glial fibrillary acidic protein (GFAP; a marker of hepatic myofibroblasts or stellate cells)[30] was included because of the canonical pathway hepatic stellate cell activation that was identified by MEA. In addition, lymphatic vessel endothelial hyaluronan receptor 1 (LYVE1) was included because it was one of the top 10 significantly

upregulated genes in FECD when compared with controls according to MEA (fold regulation = 31.68, $P = 0.003$) and confirmed by RT-qPCR (fold regulation = 39.87, $P = 0.046$). Because LYVE1 can be expressed by macrophages,[31] we wanted to check whether it was also expressed by circulating fibrocytes (or derivatives) in FECD. Finally, we included antibodies directed to CD1a (marker for dendritic Langerhans cells in the corneal epithelium, $n = 3$)[32] and T cell markers CD4 ($n = 2$) and CD8 ($n = 1$), for which no immunoreactivity was observed in FECD specimens.

Circulating fibrocytes/dendritic derivatives were present in all of the 48 tested FECD samples. No difference in number of circulating fibrocytes/dendritic derivatives was observed in phakic versus pseudophakic eyes with FECD. None of the normal controls contained such cells. Sample sizes per antiserum are given in Figure 6b for FECD. For normal controls, the sample sizes were CD45, $n = 10$; αSMA, $n = 9$; HLA-DRA, $n = 7$; collagen I, $n = 2$; CD34, $n = 1$; CD11b, $n = 1$; CCR5, $n = 1$; and LYVE1, $n = 1$.

Figure 6 summarizes the protein expression profile per cell morphology and per localization within the CE layer and gives the average number of immunoreactive cells per mm^2 of CE for each of the markers. On pure morphology, we observed a subset of cells with dendritic morphology and elongated nuclei and a smaller subset of monocyte-like cells with bean-shaped nuclei lacking dendritic processes. There were also cells of intermediate phenotype, with bean-shaped nuclei and wider cytoplasm, but without clear dendritic processes, suggesting a continuum between both subsets of cells. With respect to protein expression profile, the markers CD45, CD34, CD11b, collagen I, CCR5, CXCR2, and MMP9 were most prominent in
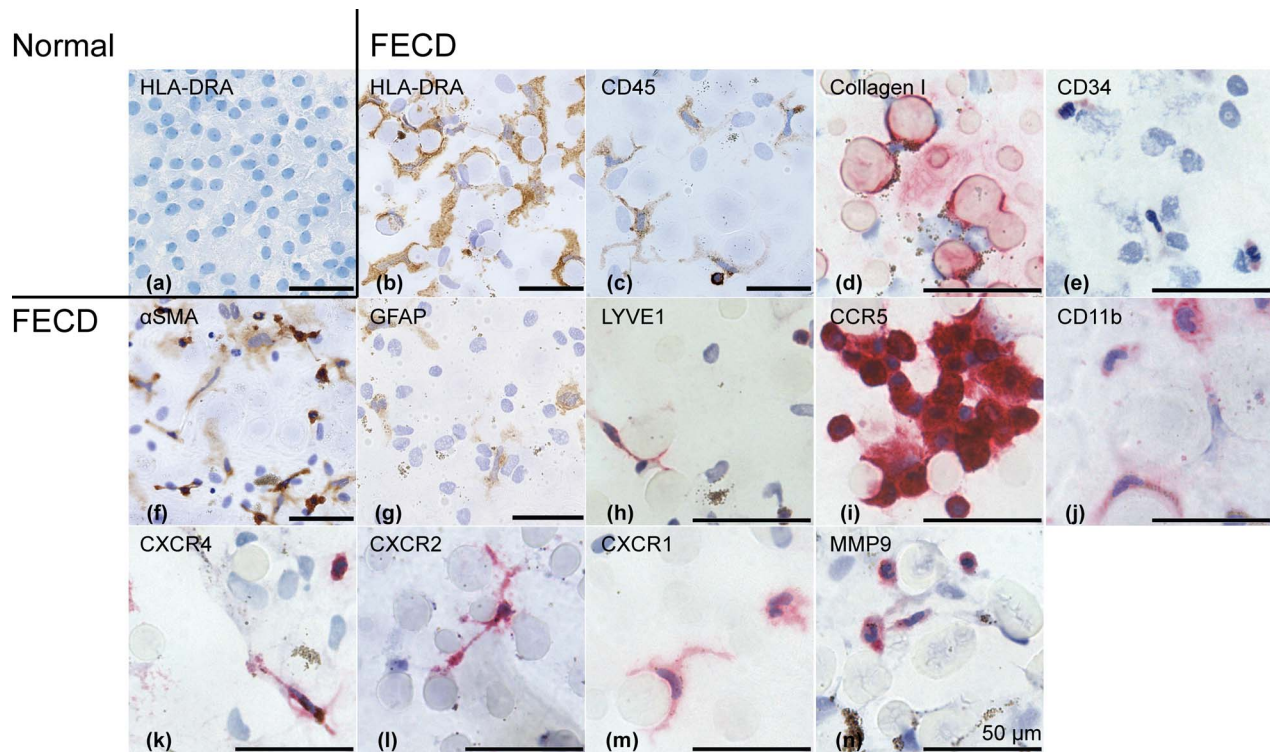
FIGURE 3. Immunohistochemistry on CE-DM complexes reveals cells with dendritic morphology in FECD. (**a-b**) HLA-DRA (*brown*) showed cells with dendritic processes that cluster around guttae, as if embracing them, in CE-DM complexes with FECD. No such cells were present in normal CE samples. (**c**) CD45 (*brown*) moderately stained cells with dendritic morphology and strongly stained a smaller subset of monocyte-like cells (rounded with bean-shaped nuclei) in CE-DM complexes with FECD. (**d, e, g–n**) Cells with dendritic/monocyte-like morphology also expressed collagen I (*red*), CD34 (*red*), GFAP (*brown*), LYVE1 (*red*), CCR5 (*red*), CD11b (*red*), CXCR4 (*red*), CXCR2 (*red*), CXCR1 (*red*), and MMP9 (*red*). (**f**) Alpha-SMA (*brown*), strongly stained cells with dendritic morphology and moderately stained CECs in CE-DM complexes with FECD. (**i**) The image for CCR5 shows incidental aggregation of monocyte-like cells in a CE-DM specimen with FECD.

the monocyte-like subset, whereas HLA-DRA, GFAP, CXCR4, and CXCR1 were most prominent in the dendritic subset of cells. LYVE1 was expressed by both subsets, again suggesting a common origin between the cells with monocyte-like and dendritic morphology. With respect to localization, the monocyte-like subset was mostly observed in the peripheral zone of the CE layer, whereas the dendritic subset was mostly observed in the center, and cells of intermediate phenotype were concentrated at the interface between the central confluency of guttae and the peripheral remaining CECs. HLA-DRA was the most prevalent marker, with a weighted average of 17.60 cells per mm^2 of CE (Fig. 6b). Thus, on an average whole mount of 42 mm^2 (7–8 mm in diameter), more than 700 HLA-DRA$^+$ cells were present. Not a single FECD sample ($n = 11$) lacked HLA-DRA$^+$ cells, and not a single control sample ($n = 7$) contained HLA-DRA$^+$ cells.

## DISCUSSION

MEA with IPA analysis ($n = 4$ FECD, $n = 4$ normal) was validated on a larger independent set of samples with RT-qPCR ($n = 9$ FECD, $n = 8$ normal) and led to the immunohistological identification of circulating fibrocytes and dendritic derivatives in the CE layer patients with FECD ($n = 48$ FECD, $n = 15$ normal). The coexpression of CD34 and CD45 respectively with collagen I proved their circulating fibrocyte identity,[25] a cell type that causes fibrosis in a variety or organs throughout the body[25,33] but that has not previously been described in FECD. Circulating fibrocytes/dendritic derivatives were present in all examined FECD samples (ranging from clinical

stages II to IV),[2] irrespective of prior cataract surgery (which is usually performed prior to endothelial keratoplasty).

Circulating fibrocytes are considered to be derived from the monocyte/macrophage lineage (with characteristic bean-shaped nuclei) because they express monocyte surface markers such as CD11b.[26] They should not be confused with bone marrow–derived mesenchymal stem cells (which have been reported to improve corneal recovery via anti-inflammatory mechanisms), which by definition do not express hematopoietic markers such as CD45, CD34, and CD11b or HLA-DR.[34–37] Circulating fibrocytes are recruited from the blood to peripheral sites of injury via chemokine ligand/ chemokine receptor axes, such as chemokine C-X-C motif ligand 12 and receptor 4 (CXCL12/CXCR4).[25,33] Upon arrival, they penetrate the site of injury and can differentiate into a variety of phenotypes related to their mixed hematopoietic character (cytokine producing or antigen presenting) and mesenchymal character (ECM producing).[25] They can enhance physiologic wound healing or cause pathologic fibrosis.[27]

It is tempting to think that the observed cells with dendritic morphology are merely CECs with degenerative changes or CECs that have become myofibroblast-like through the process of EMT.[38] However, the expression of CD45 (a cell-lineage marker of bone marrow–derived hematopoietic cells that cannot be acquired by nonhematopoietic cells, not even during EMT),[22–24] strongly pleads against this hypothesis. Furthermore, the bean-shaped nuclei are characteristic of cells from the monocyte lineage, as are circulating fibrocytes. Nevertheless, our data also support the process of EMT in FECD, consistent with current literature (Supplementary Table S2). We did not observe an upregulation of the EMT-inducing
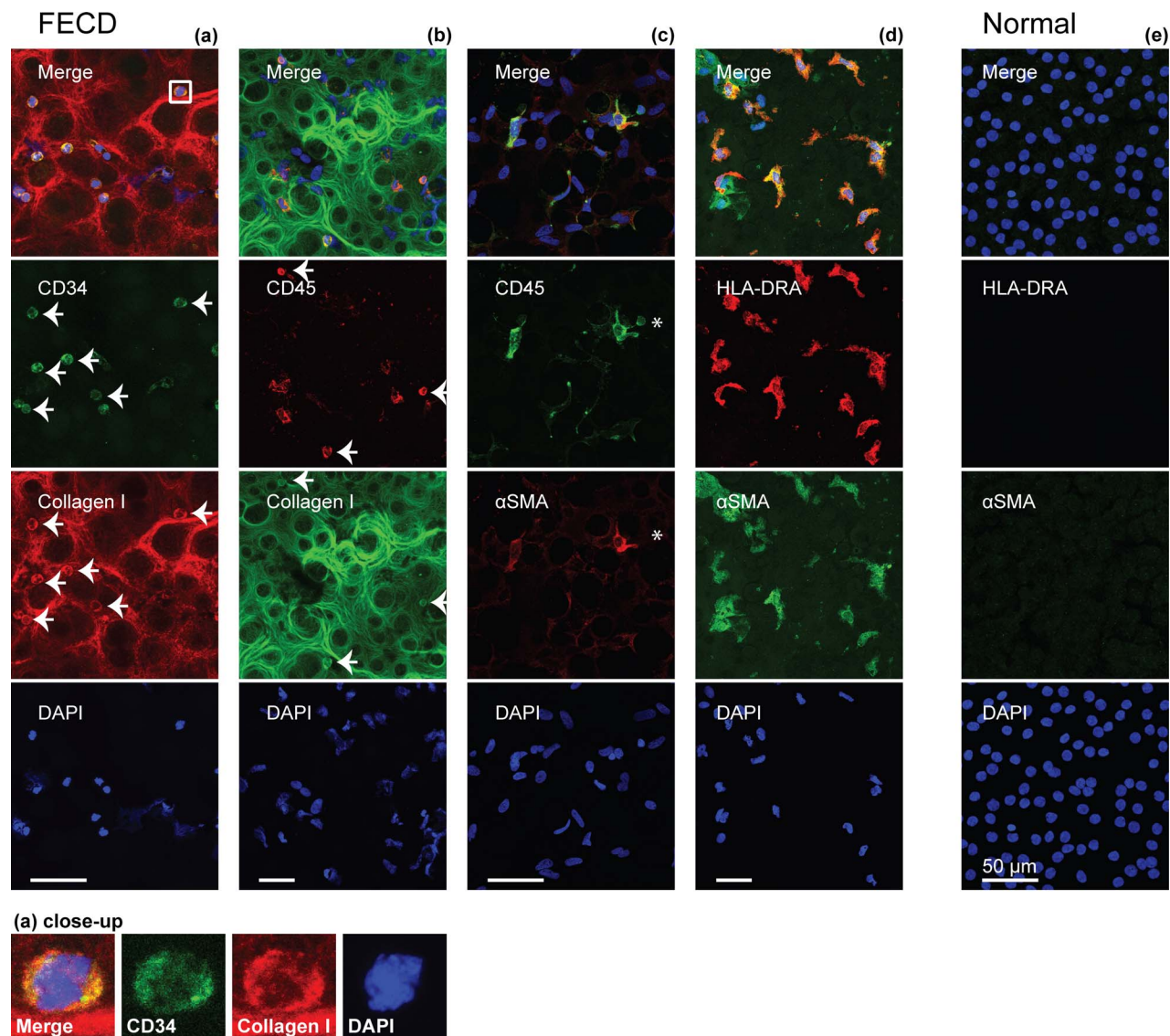
FIGURE 4. Coexpression of CD34 or CD45 with collagen I identifies circulating fibrocytes in FECD. (**a, b**) IF double stains revealed CD34^{+}/collagen I^{+} (**a**) and CD45^{+}/collagen I^{+} (**b**) cells with bean-shaped nuclei, corresponding to circulating fibrocytes in CE of patients with FECD. Samples (**a**) and (**d**) originated from phakic eyes from two different patients with FECD, indicating that the presence of cells with monocyte-like (**a**) and dendritic morphology (**d**) is not secondary to cataract surgery. A close-up of a cell with circulating fibrocyte signature (*white* rectangle in merged pannel [**a**]) is given at the *bottom* of the figure. Note the concentric deposition of collagen I fibers around guttae (*black* spots) in (**a**) and (**b**). (**c, d**) Dendritic myofibroblast-like cells (CD45^{+}/αSMA^{+}/HLA-DRA^{+}) are present in FECD and surround guttae. Occasionally, monocyte-like CD45^{+} cells (* in [**c**]) are close to cells with dendritic morphology. (**d**) Alpha-SMA is expressed by cells with dendritic morphology and CECs. (**e**) No circulating fibrocytes or cells with dendritic morphology were observed in normal CE. Each column (**a–e**) represents one sample, with the merged image at the top, and the composing channels underneath. *Yellow* indicates coexpression of *green* and *red* fluorescently labeled antigens.

genes *ZEB1* and *SNAI1*, as reported by Okumura et al.,[39] who studied the EMT profile in immortalized CECs from late-onset FECD, but we did observe a significant upregulation of *ZEB2* in FECD versus normal as reported earlier in a conference poster of the same group (Ho L, et al. *IOVS* 2013;54:ARVO E-Abstract 1680). Differences in these results might be a result of the difference between in vivo and in vitro (without circulating fibrocytes) gene expression and to the use of *GAPDH* as a reference gene for normalization (as discussed later). In contrast to Hidayat and Cockerham[38] but in line with the role of EMT in FECD,[11] we observed diffuse αSMA expression in the CE layer of patients with FECD (Fig. 4d) using two different antisera (Supplementary Table S1) with proper internal and external controls and consistent with the upregulation of

ACTA2 at the gene expression level (fold regulation = 3.69, P = 0.025, according to RT-qPCR).

Rather than being mutually exclusive, our data suggest that both processes (EMT and circulating fibrocytes) play a role in FECD. Notably, EMT and circulating fibrocytes are frequently reported to contribute simultaneously to tissue fibrosis, whereby EMT is suggested to occur in later stages (contributing to the irreversible progression of fibrosis) and circulating fibrocytes would be present in earlier stages.[40] Further study of the interplay of both processes would certainly be of interest to elucidate the pathogenesis of FECD.

When comparing our gene expression results with existing literature (Supplementary Table S2), our data confirm the significant upregulation of extracellular matrix genes agrin, collagens (*COL1A1, COL4A3, COL4A4, COL4A5, COL4A6,*
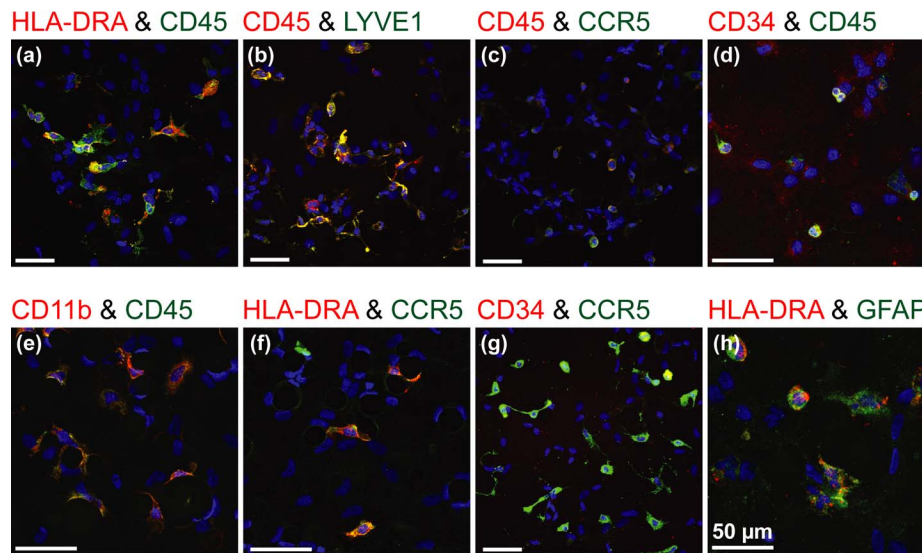
FIGURE 5. Immunofluorescent coexpression of circulating fibrocyte markers in CE of patients with FECD. Expression of CD45 is observed in monocyte-like cells, coexpressing CCR5 (**c**), CD34 (**d**), CD11b (**e**), and collagen I (Fig. 4b) and in cells with dendritic morphology, coexpressing HLA-DRA (**a**) and αSMA (Fig. 4c). Coexpression of CD45 and LYVE1 (**b**) was seen in cells of both morphologies. This suggests that both morphological subsets represent different differentiation stages of circulating fibrocytes. Sample (**c**) originates from a phakic eye with FECD, indicating that the presence of (CD45+/CCR5+) cells with monocyte-like morphology in FECD is not secondary to cataract surgery. (**c**, **f**, **g**) The expression of chemokine C-C motif 5 (CCR5) suggests that this receptor might play a role in recruitment of circulating fibrocytes to the CE layer in FECD. (**h**) Coexpression of HLA-DRA and GFAP was observed in cells with dendritic and intermediate morphology.

COL5A1, COL6A2), and fibronectin, and the significant downregulation of ribonuclease *DICER1* (involved in miRNA biogenesis) in FECD versus normal, as reported in literature.[39,41–43] In contrast with existing literature,[41,44,45] we found a significant downregulation of clusterin (*CLU*), integrins *ITGA3 and ITGB3*, MMPs (*MMP10 and MMP14*), transforming growth factor beta induced and tissue inhibitor of metalloproteinase *TIMP1* in FECD versus normal. The upregulation of extracellular matrix molecules (agrin, collagens, and fibronectin) and the downregulation of matrix-degrading molecules (MMPs, which notably degrade agrin) are consistent with the thickening of the DM in FECD. Furthermore, agrin is a critical signal for hematopoietic niches,[46] and its upregulation might be related to the presence of circulating fibrocytes in FECD. The downregulation of integrins (cell adhesion molecules) and *CLU* (prosurvival factor) is compatible, respectively, with dysfunctioning and apoptosis of CE in FECD. With respect to Du et al.,[47] who studied differential splicing events in FECD versus normal, we cannot directly compare our results because we studied gene expression irrespective of splicing variants. However, our data show a significant upregulation of EMT-related genes *CSNK1G3* and *PPFIBP1*, and no differential expression of splicing regulators *MBNL1* and *MBNL2*. With respect to oxidative stress genes, our data confirm the significant downregulation of superoxide dismutase *SOD2* and heme oxygenase *HMOX1*, as reported by Jurkunas et al.[48] In addition, we observed a significant downregulation of *SOD3* and a significant upregulation of NADPH oxidase activator *NCF2* in FECD versus normal. With respect to senescence genes, our data confirm the significant upregulation of *ARHGAP18*, *CCND1*, *CDK6*, *CDKN2A*, *CDKN2B*, *IGF1*, *IGFBP5*, *IGFBP7*, *IRF5*, *NOX4*, and *PIK3CG* in FECD versus normal, as reported by Matthaei et al.[42] However, aldehyde dehydrogenase *ALDH1A3*, which was found to be significantly upregulated in their study,[42] was significantly downregulated in our data, together with dehydrogenases *AKR1C2* and *ALDH3A1*, which were also reported to be downregulated in a serial analysis of gene expression experiment by Gottsch et al.[49] Several other genes that were upregulated according to a serial
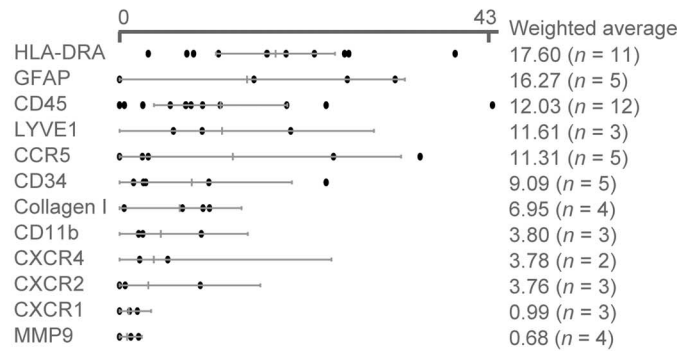
analysis of gene expression (apolipoprotein D, metallothionein *MT2A*, and serum amyloid genes *SAA1* and *SAA2*)[49] were significantly downregulated in our data; and the reverse was true for activator protein 1 transcription factor subunit *FOSB* and ion transporter *SLC4A11*. These differences in results could be a result of differences in FECD stages, that is, the patients examined with a serial analysis of gene expression were derived from penetrating keratoplasty surgery, whereas our samples were derived from endothelial keratoplasty (penetrating keratoplasty is usually performed in later stages than endothelial keratoplasty). Furthermore, others did not find a significant difference in gene expression for *SLC4A11* between FECD and normal,[50] and they argued that expression levels of ion transporters could be increased in the early stages of FECD. Apart from *FOSB*, another activator protein 1 transcription factor subunit, namely *JUN*, was also significantly upregulated in our data, consistent with the current literature.[50,51] With respect to unfolded protein response, our data confirm a significant downregulation of prefoldin subunit 5, as reported by Jalimarada et al.[50] As a last remark, differences in gene expression levels between studies can also be a result of the use of different reference genes for normalization. *GAPDH*, a frequently used reference gene,[39,41] is unstably expressed in FECD versus normal (significantly upregulated in our study and significantly downregulated in other studies[48,49]) and is therefore not the best reference gene to study gene expression in FECD.[52] We have selected *RPL13A*, *RPL19* and *RPS5* as reference genes (over *GAPDH*, *ACTB* and *HPRT1*) because of their stable expression in FECD and normal. *RPL13A* was also used by others[48,50] because of its small difference in expression between FECD and control groups.

A limitation to this study is that the samples used for MEA and RT-qPCR experiments were not matched for age and sex. However, despite this limitation, the MEA and RT-qPCR results led to the identification of circulating fibrocytes and dendritic derivatives in FECD using immunohistology on whole-mount samples that were matched for age and sex within the constraints of sample availability (FECD exhibits a female predominance and late onset,[1,4] whereas donor corneas
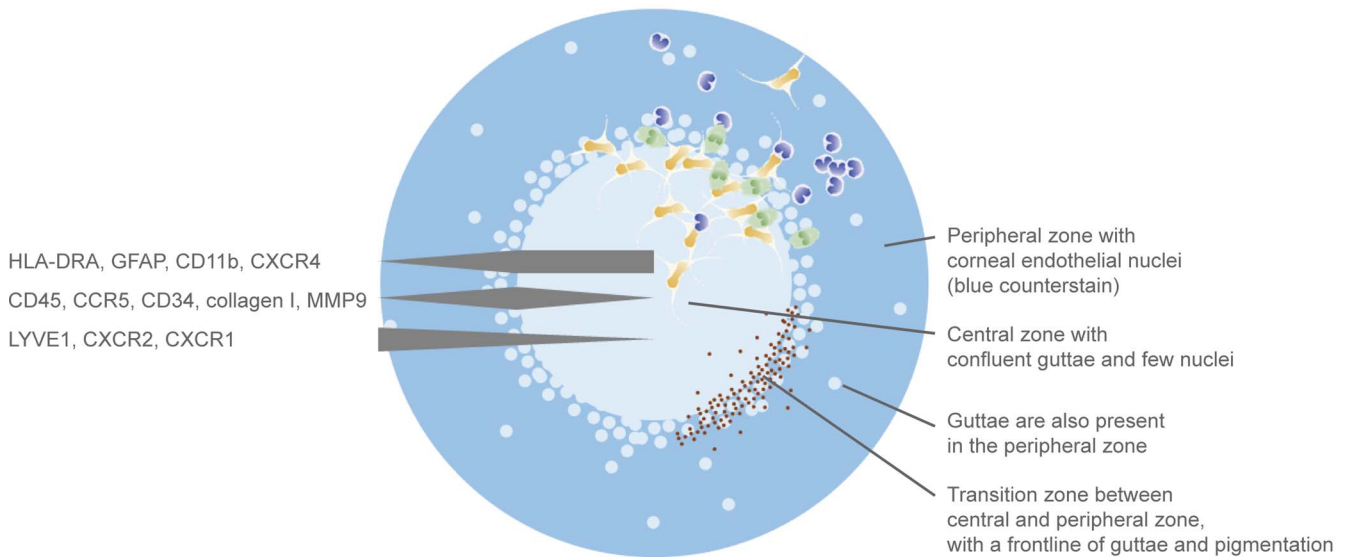
(a) Markers of cells with fibrocyte / dendritic morphology in FECD

Gutta

CD45, CCR5, collagen I, CD11b

CD34, CXCR2, MMP9

HLA-DRA, GFAP, CXCR4, CXCR1

LYVE1
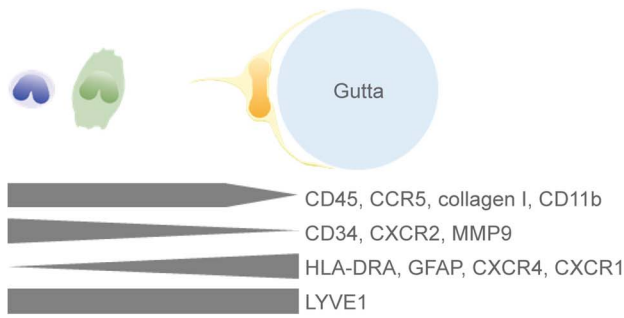
(b) Number of cells expressing a protein of interest per mm² of corneal endothelium in FECD

	0	43	Weighted average
HLA-DRA			17.60 ($n = 11$)
GFAP			16.27 ($n = 5$)
CD45			12.03 ($n = 12$)
LYVE1			11.61 ($n = 3$)
CCR5			11.31 ($n = 5$)
CD34			9.09 ($n = 5$)
Collagen I			6.95 ($n = 4$)
CD11b			3.80 ($n = 3$)
CXCR4			3.78 ($n = 2$)
CXCR2			3.76 ($n = 3$)
CXCR1			0.99 ($n = 3$)
MMP9			0.68 ($n = 4$)

(c) Localization of cells with fibrocyte / dendritic morphology and localization of markers in corneal endothelial whole mounts from patients with FECD

HLA-DRA, GFAP, CD11b, CXCR4

CD45, CCR5, CD34, collagen I, MMP9

LYVE1, CXCR2, CXCR1

Peripheral zone with corneal endothelial nuclei (blue counterstain)

Central zone with confluent guttae and few nuclei

Guttae are also present in the peripheral zone

Transition zone between central and peripheral zone, with a frontline of guttae and pigmentation

FIGURE 6. Protein expression profile, number, and localization of cells with monocyte-like or dendritic morphology in FECD. (**a**) Protein expression profiles per cell morphology. Cells ranged from small and round with bean-shaped nucleus (*blue*, monocyte-like morphology) to larger, plump cells with abundant cytoplasm and a similar nucleus (*green*, intermediate morphology), to cells with long dendritic processes and slender elongated nucleus (*yellow*, dendritic morphology). Antibodies to CD45, CCR5, collagen I, CD11b, CD34, CXCR2, and MMP9 marked the cells with monocyte-like morphology, whereas staining for HLA-DRA, GFAP, CXCR4, and CXCR1 marked the cells with dendritic morphology. LYVE1 was present in both morphological subsets of cells. (**b**) Number of cells expressing a protein of interest (irrespective of cell morphology) per mm² of CE in FECD. HLA-DRA was the most prominent and frequently expressed marker for cells with dendritic morphology, with a weighted average of 17.60 cells/mm². Cells expressing HLA-DRA, CD45, CD34, collagen I, αSMA, LYVE1, CD11b, and CXCR4 were present in every tested specimen ($n = 3–12$), whereas variable expression was seen for MMP9 (positive in 2/4 specimens), GFAP (positive in 4/5 specimens), CCR5 (positive in 4/5 specimens), CXCR2 (positive in 2/3 specimens), and CXCR1 (positive in 2/3 specimens). *Error bars*: mean with 95% confidence interval. *n*: sample size. (**c**) Localization of cells with different morphologies and localization of markers (irrespective of morphology) within the CE layer of patients with FECD. In the transition zone between the central confluency of guttae and the peripheral remaining CECs, cells with intermediate morphology were most prominent, coinciding with the expression of CD45, CCR5, CD34, collagen I, and MMP9. In the central zone, cells with dendritic morphology prevailed, coinciding with the expression of HLA-DRA, GFAP, CD11b, and CXCR4. In the peripheral zone, cells with monocyte-like morphology prevailed, coinciding with the expression of LYVE1, CXCR2, and CXCR1. This figure is complementary, but not identical to (**a**), as illustrated by the fact that CXCR1 immunoreactivity was mostly observed in the peripheral zone (**c**), in cells with dendritic morphology (**a**). CD11b was mostly observed in the central zone (**c**) in cells with monocyte-like morphology (**a**). Alpha-SMA, fibronectin, and vimentin were not included in this figure because they were also expressed by CECs.

overrepresent younger and male individuals). This finding was novel and consistent.

The fact that these cells have not been described previously despite advanced techniques such as confocal laser scanning microscopy can be explained by their relatively low numbers and their morphology. Circulating fibrocytes are typically described as spindle shaped, compatible with the morphology of cells in our samples with intermediate and dendritic morphology, when these would be cross-sectioned. Full-thickness cross-sections were not suited to detect cells with dendritic morphology. Also, on CE-DM whole mounts they could only be detected using specific markers for circulating fibrocytes. Sampling problems also arise because only an estimated 700 HLA-DRA⁺ cells with dendritic morphology (1.4% of cells in a layer containing 50,400 remaining CECs at 1200 cells/mm²)[3] and <300 collagen I⁺ cells with monocyte-

like morphology (<0.6% of the total cell number) are present in an average CE-DM specimen of 42 mm^2. Furthermore, these cells cover a broad spectrum of morphologies and marker combinations, depending on their differentiation state (from cells with monocyte-like morphology to myofibroblast-like cells with dendritic morphology), similar to what has been reported in other fibrosing disorders that involve circulating fibrocytes.[40] These small numbers and diverse phenotypes would also make it difficult to isolate them from the CE layer for in vitro studies on their recruitment and exact function in FECD. Alternatively, circulating fibrocytes could be isolated from the peripheral blood, similar to what has been done for other fibrosing disorders.[53]

With respect to the recruitment of circulating fibrocytes toward the CE layer in FECD, our mRNA data suggest a role for chemokine receptors *CCR5* (RT-qPCR fold regulation = 10,84, $P = 0.019$; Figs. 3i, 5c, 5f, 5g, 6), *CCR1* (MEA fold regulation = 3.62, $P = 0.036$; RT-qPCR fold regulation = 10.05, $P = 0.042$), and *CX3CR1* (MEA fold regulation = 10.32, $P = 0.003$; RT-qPCR fold regulation = 4.92, $P = 0.017$). The differential localization of cells with different morphology in the CE layer of patients with FECD (Fig. 6c) suggests that circulating fibrocytes enter the CE layer peripherally, where we observed the monocyte-like subset of cells (with rounded contours, consistent with a recent exit from the circulation), and differentiate into larger dendritic myofibroblast-like cells toward the center. Therefore, we speculate that circulating fibrocytes might enter the anterior eye chamber by extravasation from blood vessels in the iris-ciliary body, as is common during intraocular inflammation,[54] or via the trabecular meshwork, where rare CD45$^+$ dendritic cells coexpressing monocyte markers have been reported.[55] Although FECD is not accompanied by overt ocular inflammation, a process of para-inflammation might be active, similar to other age-associated degenerative diseases of the immunoprivileged eye (such as adult macular degeneration, glaucoma, and diabetic retinopathy), which might allow circulating fibrocytes to enter the anterior chamber.[56] Further research is needed to study the recruitment of circulating fibrocytes to the CE layer in FECD.

Based on this observational study, we cannot conclude on the exact function of circulating fibrocytes/dendritic derivatives in FECD. However, these cells are known to cause organ fibrosis in a variety of disorders, including autoimmune diseases, such as scleroderma, and chronic inflammatory disorders that are not classically thought of as autoimmune, such as idiopathic pulmonary fibrosis, renal fibrosis, liver fibrosis, and proliferative retinopathy.[25,33,53] Similarly, circulating fibrocytes might contribute to the deposition of ECM that is characteristic for FECD. If so, they might be a valuable novel target for the development of nonsurgical therapy. Moreover, patients with FECD might benefit from therapies that are being developed for organ fibrosis,[57,58] such as CCR1 antagonists (inhibit circulating fibrocyte trafficking),[40] angiotensin II type 1 receptor inhibitors (inhibit fibrogenesis),[40] and injections of serum amyloid P (inhibit fibrocyte differentiation).[59] Notably, ROCK-inhibitors, which are currently tested to treat edematous corneas,[60] might also act on the activity of circulating fibrocytes via the TGFβ1 pathway, as TGFβ1 is not only an inducer of EMT[40] but also an inducer of differentiation of circulating fibrocytes into (myo)fibroblast-like cells.[33]

Another question that is raised by these data is whether circulating fibrocytes/dendritic derivatives play a primary or secondary role in FECD. In this noninterventional study, we only had access to specimens from symptomatic cases of FECD (clinical stages II to IV),[2] which were collected as residual human explant material from therapeutic endothelial kerato-plasty. We detected circulating fibrocytes/dendritic derivatives in all symptomatic stages of FECD, but we cannot conclude on

their presence in (asymptomatic) stage I of FECD, which would require an interventional study approach. In a future study we will use RNA-sequencing and IHC to compare corneas with FECD to normal and to a third group of edematous corneas without FECD (such as pseudophakic bullous keratopathy and endothelial graft failure). This will shed light on the specificity of circulating fibrocytes in the pathogenesis of FECD. However, even if the recruitment of these cells would be a common secondary reaction in CE disorders, they might still qualify as drug targets to halt disease progression (hypothetically even in a variety of CE disorders), and their presence refutes the former dogma that no inflammatory cells are present within the CE layer of patients with FECD.[4] Further study would then be required to characterize their recruitment, differentiation, and function in different CE disorders.

In conclusion, circulating fibrocytes and their dendritic derivatives are a novel and consistent aspect of symptomatic FECD. Their presence should be taken into account in all future studies that investigate the CE layer of patients with FECD. Their recruitment, differentiation, and function in FECD deserve further investigation because these insights might present new therapeutic avenues for patients with FECD.

Disclosure: **A.-K. De Roo**, None; **J. Wouters**, None; **O. Govaere**, None; **B. Foets**, None; **J.J. van den Oord**, None

References

1. Elhalis H, Azizi B, Jurkunas UV. Fuchs endothelial corneal dystrophy. *Ocul Surf*. 2010;8:173–184.

2. Suh LH, Emerson MV, Jun AS. Cornea and external eye disease—corneal allotransplantation, allergic disease and trachoma. In: Reinhard T, Larkin F, eds. *Essentials in Ophthalmology*. Berlin Heidelberg: Springer-Verlag; 2008:1–13.

3. Eghrari AO, Gottsch JD. Fuchs' corneal dystrophy. *Expert Rev Ophthalmol*. 2010;5:147–159.

4. Zhang J, Patel DV. The pathophysiology of Fuchs' endothelial dystrophy—a review of molecular and cellular insights. *Exp Eye Res*. 2015;130:97–105.

5. Zhu AY, Eberhart CG, Jun AS. Fuchs endothelial corneal dystrophy: a neurodegenerative disorder? *JAMA Ophthalmol*. 2014;132:377–378.

6. Joyce NC. Proliferative capacity of corneal endothelial cells. *Exp Eye Res*. 2012;95:16–23.

7. Wright AF, Dhillon B. Major progress in Fuchs's corneal dystrophy. *N Engl J Med*. 2010;363:1072–1075.

8. Zhang X, Igo RP Jr, Fondran J, et al. Association of smoking and other risk factors with fuchs' endothelial corneal

Investigative Ophthalmology & Visual Science

dystrophy severity and corneal thickness. *Invest Ophthalmol Vis Sci*. 2013;54:5829–5835.

9. Schmedt T, Silva MM, Ziaei A, Jurkunas U. Molecular bases of corneal endothelial dystrophies. *Exp Eye Res*. 2012;95:24–34.

10. Vasanth S, Eghrari AO, Gapsis BC, et al. Expansion of CTG18.1 trinucleotide repeat in TCF4 is a potent driver of Fuchs' corneal dystrophy. *Invest Ophthalmol Vis Sci*. 2015;56:4531–4536.

11. Okumura N, Minamiyama R, Ho LT, et al. Involvement of ZEB1 and Snail1 in excessive production of extracellular matrix in Fuchs endothelial corneal dystrophy. *Lab Invest*. 2015;95:1291–1304.

12. Poulsen ET, Dyrlund TF, Runager K, et al. Proteomics of Fuchs' endothelial corneal dystrophy support that the extracellular matrix of Descemet's membrane is disordered. *J Proteome Res*. 2014;13:4659–4667.

13. Eye Bank Association of America. Eye Banking Statistical Report. Washington, DC: Eye Bank Association of America, 2014.

14. Tan DT, Dart JK, Holland EJ, Kinoshita S. Corneal transplantation. *Lancet*. 2012;379:1749–1761.

15. Smyth GK. Linear models and empirical bayes methods for assessing differential expression in microarray experiments. *Stat Appl Genet Mol Biol*. 2004;3: Article 3.

16. Benjamini Y, Hochberg Y. Controlling the false discovery rate: a practical and powerful approach to multiple testing. *J R Stat Soc Series B Stat Methodol*. 1995;57:289–300.

17. Schindelin J, Arganda-Carreras I, Frise E, et al. Fiji: an open-source platform for biological-image analysis. *Nat Methods*. 2012;9:676–682.

18. Kim CC, Derisi JL. VersaCount: customizable manual tally software for cell counting. *Source Code Biol Med*. 2010;5:1.

19. Tacke F, Zimmermann HW. Macrophage heterogeneity in liver injury and fibrosis. *J Hepatol*. 2014;60:1090–1096.

20. Subramanian A, Tamayo P, Mootha VK, et al. Gene set enrichment analysis: a knowledge-based approach for interpreting genome-wide expression profiles. *Proc Natl Acad Sci U S A*. 2005;102:15545–15550.

21. Edgar R, Domrachev M, Lash AE. Gene Expression Omnibus: NCBI gene expression and hybridization array data repository. *Nucleic Acids Res*. 2002;30:207–210.

22. Hermiston ML, Xu Z, Weiss A. CD45: a critical regulator of signaling thresholds in immune cells. *Annu Rev Immunol*. 2003;21:107–137.

23. Kallergi G, Papadaki MA, Politaki E, Mavroudis D, Georgoulias V, Agelaki S. Epithelial to mesenchymal transition markers expressed in circulating tumour cells of early and metastatic breast cancer patients. *Breast Cancer Res*. 2011;13:R59.

24. Giordano A, Gao H, Anfossi S, et al. Epithelial-mesenchymal transition and stem cell markers in patients with HER2-positive metastatic breast cancer. *Mol Cancer Ther*. 2012;11:2526–2534.

25. Herzog EL, Bucala R. Fibrocytes in health and disease. *Exp Hematol*. 2010;38:548–556.

26. Lin RJ, Su ZZ, Liang SM, et al. Role of circulating fibrocytes in cardiac fibrosis. *Chin Med J (Engl)*. 2016;129:326–331.

27. Suga H, Rennert RC, Rodrigues M, et al. Tracking the elusive fibrocyte: identification and characterization of collagen-producing hematopoietic lineage cells during murine wound healing. *Stem Cells*. 2014;32:1347–1360.

28. Eghrari AO, Riazuddin SA, Gottsch JD. Fuchs corneal dystrophy. *Prog Mol Biol Transl Sci*. 2015;134:79–97.

29. Merjava S, Neuwirth A, Mandys V, Jirsova K. Cytokeratins 8 and 18 in adult human corneal endothelium. *Exp Eye Res*. 2009;89:426–431.

30. Okamoto K, Tajima H, Ohta T, et al. Angiotensin II induces tumor progression and fibrosis in intrahepatic cholangiocarcinoma through an interaction with hepatic stellate cells. *Int J Oncol*. 2010;37:1251–1259.

31. Schroedl F, Brehmer A, Neuhuber WL, Kruse FE, May CA, Cursiefen C. The normal human choroid is endowed with a significant number of lymphatic vessel endothelial hyaluronate receptor 1 (LYVE-1)-positive macrophages. *Invest Ophthalmol Vis Sci*. 2008;49:5222–5229.

32. Mayer WJ, Irschick UM, Moser P, et al. Characterization of antigen-presenting cells in fresh and cultured human corneas using novel dendritic cell markers. *Invest Ophthalmol Vis Sci*. 2007;48:4459–4467.

33. Mattoli S, Bellini A, Schmidt M. The role of a human hematopoietic mesenchymal progenitor in wound healing and fibrotic diseases and implications for therapy. *Curr Stem Cell Res Ther*. 2009;4:266–280.

34. Uccelli A, Moretta L, Pistoia V. Mesenchymal stem cells in health and disease. *Nat Rev Immunol*. 2008;8:726–736.

35. Vemuri MC, Chase LG, Rao MS. Mesenchymal stem cell assays and applications. *Methods Mol Biol*. 2011;698:3–8.

36. Li F, Zhao SZ. Control of cross talk between angiogenesis and inflammation by mesenchymal stem cells for the treatment of ocular surface diseases. *Stem Cells Int*. 2016;2016:7961816.

37. Ko JH, Lee HJ, Jeong HJ, et al. Mesenchymal stem/stromal cells precondition lung monocytes/macrophages to produce tolerance against allo- and autoimmunity in the eye. *Proc Natl Acad Sci U S A*. 2016;113:158–163.

38. Hidayat AA, Cockerham GC. Epithelial metaplasia of the corneal endothelium in Fuchs endothelial dystrophy. *Cornea*. 2006;25:956–959.

39. Okumura N, Minamiyama R, Ho LT, et al. Involvement of ZEB1 and Snail1 in excessive production of extracellular matrix in Fuchs endothelial corneal dystrophy. *Lab Invest*. 2015;95:1291–1304.

40. Liu Y. Cellular and molecular mechanisms of renal fibrosis. *Nat Rev Nephrol*. 2011;7:684–696.

41. Weller JM, Zenkel M, Schlotzer-Schrehardt U, Bachmann BO, Tourtas T, Kruse FE. Extracellular matrix alterations in late-onset Fuchs' corneal dystrophy. *Invest Ophthalmol Vis Sci*. 2014;55:3700–3708.

42. Matthaei M, Zhu AY, Kallay L, Eberhart CG, Cursiefen C, Jun AS. Transcript profile of cellular senescence-related genes in Fuchs endothelial corneal dystrophy. *Exp Eye Res*. 2014;129:13–17.

43. Matthaei M, Hu J, Kallay L, et al. Endothelial cell microRNA expression in human late-onset Fuchs' dystrophy. *Invest Ophthalmol Vis Sci*. 2014;55:216–225.

44. Jurkunas UV, Bitar MS, Rawe I, Harris DL, Colby K, Joyce NC. Increased clusterin expression in Fuchs' endothelial dystrophy. *Invest Ophthalmol Vis Sci*. 2008;49:2946–2955.

45. Jurkunas UV, Bitar M, Rawe I. Colocalization of increased transforming growth factor-beta-induced protein (TGFBIp) and Clusterin in Fuchs endothelial corneal dystrophy. *Invest Ophthalmol Vis Sci*. 2009;50:1129–1136.

46. Mazzon C, Anselmo A, Cibella J, et al. The critical role of agrin in the hematopoietic stem cell niche. *Blood*. 2011;118:2733–2742.

47. Du J, Aleff RA, Soragni E, et al. RNA toxicity and missplicing in the common eye disease fuchs endothelial corneal dystrophy. *J Biol Chem*. 2015;290:5979–5990.

48. Jurkunas UV, Bitar MS, Funaki T, Azizi B. Evidence of oxidative stress in the pathogenesis of fuchs endothelial corneal dystrophy. *Am J Pathol*. 2010;177:2278–2289.

49. Gottsch JD, Bowers AL, Margulies EH, et al. Serial analysis of gene expression in the corneal endothelium of Fuchs' dystrophy. *Invest Ophthalmol Vis Sci*. 2003;44:594–599.

50. Jalimarada SS, Ogando DG, Bonanno JA. Loss of ion transporters and increased unfolded protein response in Fuchs' dystrophy. *Mol Vis*. 2014;20:1668–1679.

51. Matthaei M, Hu J, Meng H, et al. Endothelial cell whole genome expression analysis in a mouse model of early-onset Fuchs' endothelial corneal dystrophy. *Invest Ophthalmol Vis Sci*. 2013;54:1931–1940.

52. Klenke S, Renckhoff K, Engler A, Peters J, Frey UH. Easy-to-use strategy for reference gene selection in quantitative real-time PCR experiments. *Naunyn Schmiedebergs Arch Pharmacol*. 2016;389:1353–1366.

53. Hu X, DeBiasi EM, Herzog EL. Flow cytometric identification of fibrocytes in the human circulation. *Methods Mol Biol*. 2015;1343:19–33.

54. Howes EL Jr, Cole PW, Adair TM, Cruse VK, Pollycove M. Cellular and vascular responses in acute experimental ocular inflammation. *Invest Ophthalmol Vis Sci*. 1994;35:4031–4038.

55. Flugel C, Kinne RW, Streilein JW, Lutjen-Drecoll E. Distinctive distribution of HLA class II presenting and bone marrow derived cells in the anterior segment of human eyes. *Curr Eye Res*. 1992;11:1173–1183.

56. Perez VL, Caspi RR. Immune mechanisms in inflammatory and degenerative eye disease. *Trends Immunol*. 2015;36:354–363.

57. Rockey DC. Translating an understanding of the pathogenesis of hepatic fibrosis to novel therapies. *Clin Gastroenterol Hepatol*. 2013;11:224–231.e225.

58. Craig VJ, Zhang L, Hagood JS, Owen CA. Matrix metalloproteinases as therapeutic targets for idiopathic pulmonary fibrosis. *Am J Respir Cell Mol Biol*. 2015;53:585–600.

59. Pilling D, Cox N, Vakil V, Verbeek JS, Gomer RH. The long pentraxin PTX3 promotes fibrocyte differentiation. *PLoS One*. 2015;10:e0119709.

60. Koizumi N, Okumura N, Ueno M, Kinoshita S. New therapeutic modality for corneal endothelial disease using Rho-associated kinase inhibitor eye drops. *Cornea*. 2014;33(suppl 11):S25–S31.

Investigative Ophthalmology & Visual Science